Earth's Future

Multivariate Drought Monitoring, Propagation, and Projection Using Bias-Corrected General Circulation Models

Oluwafemi E. Adeyeri[1] , Wen Zhou[2] , Patrick Laux[3] , Christopher E. Ndehedehe[4,5] , Xuan Wang[1] , Muhammad Usman[6] , and Akintomide A. Akinsanola[7,8]

[1]School of Energy and Environment, Low-Carbon and Climate Impact Research Centre, City University of Hong Kong, Kowloon, Hong Kong Special Administrative Region, [2]Department of Atmospheric and Oceanic Sciences, Institute of Atmospheric Sciences, Fudan University, Shanghai, China, [3]Institute for Meteorology and Climate Research Atmospheric Environmental Research, Karlsruhe Institute of Technology, Campus Alpine, Karlsruhe, Germany, [4]School of Environment and Science, Griffith University, Nathan, QLD, Australia, [5]Australian Rivers Institute, Griffith University, Nathan, QLD, Australia, [6]Faculty of Science Engineering and Built Environment, School of Engineering, Deakin University, Geelong, Australia, [7]Department of Earth and Environmental Sciences, University of Illinois Chicago, Chicago, IL, USA, [8]Environmental Science Division, Argonne National Laboratory, Lemont, IL, USA

Abstract Understanding how droughts are characterized, propagated, and projected, particularly multivariate droughts, is necessary to explain the variability and changes in drought characteristics. This study aims to understand multimodel global drought monitoring, propagation, and projection by utilizing a multivariate standardized drought index (MSDI) during the historical (1959–2014) and future (2045–2100) periods under two socioeconomic pathways SSPs (370 and 585), derived from the bias-corrected Coupled Model Intercomparison Project Phase 6 (CMIP6). Based on the energy metrics, the multivariate bias correction method outperformed other techniques in correcting the biases in the CMIP6 drought representation. The drought indicators demonstrate distinct categories for meteorological, hydrological, and multivariate droughts. There were significant high cross correlations between Heatwave Total Length (HWTL) and MSDI in Africa and South America for all lagged times. Europe and North America generally saw the maximum MSDI drought duration (228 months) during the historical period. For future projections, Africa recorded the maximum drought duration (197 months), while Europe witnessed the minimum drought duration for SSP 370 (171 months), and North America (149 months) for SSP 585. Furthermore, during the historical period in tropical Africa, the propagation of meteorological to hydrological drought was slower during the wet months than during the dry months. Under the SSP 370 future projection, there was a shift in the long period of meteorological-hydrological propagation from the middle and late wet months to the beginning of the wet months in tropical Africa. Therefore, tracking and projecting drought characteristics is vital for understanding the risk of drought-related consequences.

Plain Language Summary This study investigates a multimodel approach to assessing the global drought and learning more about how droughts spread, are predicted, what they look like, and their effects. Depending on the time of year, the beginning of a hydrological and multivariate drought differs from that of a meteorological drought. In general, under the medium and high socioeconomic and carbon emission scenarios, drought severity and intensity increased from the historical period to the end of the 21st century. Africa had the longest drought at the end of the 21st century (197 months). In contrast, under the medium socioeconomic and carbon emission scenarios, Europe experienced the shortest drought duration (171 months). In midlatitude Europe, the transition from a meteorological to a hydrological drought occurred slowly over the peak winter and spring months. In late summer and early fall, heatwave took an average of 1 month to propagate into hydrological drought. Future droughts are expected to be more severe for most continents. This suggests more prevalent future droughts, increasing the vulnerability of more nations to the consequences of climate change. Therefore, while creating drought preparedness, adaptation, or mitigation strategies, policymakers and planners must simultaneously consider the impacts of drought on multiple subsystems, drought propagation qualities, and regional exogenous conditions.

1. Introduction

Drought affects millions worldwide (Yuan et al., 2017). It is caused primarily by rainfall deficits, consequently impacting water availability and the productivity of freshwater ecosystems (Ault, 2020). The socioeconomic impact of droughts can increase the risk of hunger and health complications, which may ultimately lead to forced migration and even fatalities (Ngcamu & Chari, 2020).

Concurrent severe occurrences like heatwaves and meteorological droughts have increased due to global warming (AghaKouchak et al., 2014; Ballarin et al., 2021). These effects might result in prolonged and more severe hydrological droughts. Due to the projected rise in drought severity and magnitude brought on by global warming, this is expected to continue in the future (Naumann et al., 2018). Reduced stream discharge, decreased groundwater levels, and lowered reservoir storage are all critical negative impacts of drought (Adeyeri, Laux, Lawin, & Arnault, 2020; Maity et al., 2013). Drought, however, may spread at varying rates in the hydrological subsystem. Groundwater and reservoir systems can have a significant lagged response depending on factors like recharge rate. Unlike these systems, surface hydrological drainage may experience relatively rapid propagation due to water consumption, management, and climate and basin properties (Han et al., 2019; Yuan et al., 2017). These different factors could transform a hydrological drought into an agricultural and socioeconomic drought (Hao et al., 2017; Son et al., 2012).

Numerous drought indices have been developed and utilized over the past few decades to characterize various types of drought (Adeyeri et al., 2017; Ault, 2020; Fuentes et al., 2022; Ndehedehe, 2022; Ndehedehe et al., 2021). The suitability of specific drought indices depends on a particular place, season, and application. However, there are inconsistencies surrounding the widely used drought indicators (Hao et al., 2017), specifically when a drought indicator focuses on a single variable (Ndehedehe, 2022). Since drought events are connected to several variables, investigations focused on a single variable (or indicator) may not be adequate (e.g., precipitation). For instance, in the tropics, where average precipitation is relatively high, a meteorological drought (precipitation deficit) may not lead to an agricultural drought (soil moisture deficit) or hydrological drought (streamflow deficit). Many studies have utilized multivariate drought index, for example, the Multivariate Standardized Drought Index (MSDI), to circumvent this. This describes various aspects of drought from multiple perspectives for drought management and characterizes the overall or compound drought condition. For example, Hao and AghaKouchak (2013) used the MSDI based on the Standardized Precipitation Index (SPI) and the Standardized Soil Moisture Index (SSI) for drought characterization. Naderi et al. (2022) applied the Standardized Precipitation Evaporation Index (SPEI) and the SSI for the 1980–2016 and 2020–2056 periods under two climate scenarios. Xu et al. (2019) examined the propagation time between SPI and SRI in northern China. Gebrechorkos et al. (2022) characterized the streamflow drought in the Volta Basin of West Africa between 1979 and 2013. Xu et al. (2021) examined a parametric multivariate Standard Precipitation, potential Evapotranspiration, and root-zone Soil Moisture Index for drought monitoring and verified its usefulness in central China's agricultural drought early warning and recovery evaluation. Wang et al. (2020) characterized meteorological and hydrological drought using a copula-based Standardized Precipitation Evapotranspiration Streamflow Index over the Yellow River Basin of China. They further confirmed that this multivariate drought index captures the duration of drought reasonably well, affirming the Frank-copula as the best-fitted copula function for the basin. Other studies (Cheng et al., 2023; Derradji et al., 2023; Jiao et al., 2021; Mukhawana et al., 2023; Nugraha et al., 2023) categorized drought based on remote sensing approaches. Despite the importance of multivariate approaches to drought assessment (Hao & AghaKouchak, 2013), there is still a gap in the use of MSDI-based drought indicators to provide information on drought propagation and projection.

Future climate projections have been made using climate models. However, climate models and reference data do not always agree because of the differences in land surface schemes and the modeling of components (Adeyeri et al., 2022; Dieng et al., 2022). Consequently, climate change impact projections require correcting these biases (Dieng et al., 2022; Laux et al., 2021). Multivariate bias correction (BC) strategies take into account the entire multivariate dependency structure between several dependent and independent variables (Adeyeri, Laux, Lawin, & Oyekan, 2020; Dieng et al., 2022), whereas univariate BC strategies, such as quantile mapping (Adeyeri et al., 2019) or linear scaling (Laux et al., 2021; Naderi et al., 2022), map the source distribution's quantiles to the target distribution's quantiles or applies a change factor from a particular observed variable to its model simulated counterpart. For example, in the study by Naderi et al. (2022), the analysis was performed at the microscale level using climate models for drought projection. However, a change factor BC method was used in correcting the GCM

biases, and no information was provided about drought propagation. Other studies, for example (Gebrechorkos et al., 2022; Guion et al., 2022; Javed et al., 2021; Jehanzaib & Kim, 2020; Le et al., 2019; Libonati et al., 2022; Xu et al., 2019), did not give any information about drought projection. Also, they performed local-scale analysis. Additionally, a holistic evaluation of the bias correction method used in correcting General Circulation Models (GCMs) projections in drought studies is lacking (Naderi et al., 2022). Nevertheless, as the climate continues to change, it is essential to comprehensively assess drought's impact, propagation, and projections in the context of the changing climate.

Therefore, this study aims to investigate a multimodel approach to global drought assessment to improve understanding of drought propagation, projection, characteristics, and impact. To this end, a new MSDI consisting of SPI, SRI, and HWTL during historical (1959–2014) and future (2045–2100) periods under two SSPs, 370 and 585, derived from bias-corrected CMIP6, were utilized to investigate the meteorological, hydrological, and combined droughts. Unique to heatwaves is the requirement that a distinct sort of high-temperature event persists for many days. However, because specific heatwaves have a short lifespan, they may not immediately impact drought. Therefore, the HTWL considers the aggregate number of heatwaves during a specific time frame (Adeyeri et al., 2022) to account for the propagation time. Additionally, multivariate copula functions (Hao et al., 2017; Laux et al., 2011; Ma et al., 2022) were employed for combined drought modelling based on the MSDI. The multivariate drought return period was constructed based on its features using the joint probability derived from the copula functions.

The objectives of this study are to (a) bias correct GCMs for proper drought representation, (b) project drought and heatwave using the multivariate-bias-corrected CMIP6 model, and (c) examine drought and heatwave propagation and return periods for different domains.

2. Data and Methods

2.1. Data

The CMIP6 data set integrates five shared socioeconomic pathways (SSPs; Eyring et al., 2016). However, this study focuses on nine CMIP6 models and their ensemble means (Table S1 in Supporting Information S1) during the historical (1959–2014) and future (2045–2100) periods under SSP 370 and 585 scenarios. SSP 370 is the medium-to-high end of future emissions and temperature scenarios (O'Neill et al., 2016), while SSP 585 is the only SSP with emissions sufficient to deliver the 8.5 W/m^2 level of forcing in 2100 (Ndehedehe et al., 2023). The monthly reference data set for precipitation, minimum and maximum air temperature, and mean air temperature is based on the Climate Research Unit (CRU) series (Harris et al., 2020), while the reference runoff is based on the Global Runoff Ensemble (GRUN) (Ghiggi et al., 2021) at 0.5° resolution. The relative humidity and wind speed are based on the fifth-generation ECMWF atmospheric reanalysis (ERA5) (Hersbach et al., 2020) at 0.25° resolution. Many studies have ranked these data sets high in impact study assessment (Naderi et al., 2022; Xu et al., 2022). The second-order conservative mapping was used to regrid all precipitation outputs. In contrast, bilinear interpolation was used to regrid all temperature outputs (Agrafiotis, 2014), all to a typical 1° × 1° grid to prevent erroneous scale gap effects (Iturbide et al., 2022).

2.2. Standardized Drought Index (SDI)

The Univariate SDI (USDI) indices, SPI and SRI, were used to quantify meteorological and hydrological droughts, respectively. Hao et al. (2017) demonstrated that these indices satisfy several essential drought indicator characteristics, including statistical consistency and comparability at various geographical scales. MSDI examines meteorological and hydrological drought characteristics by establishing the joint distribution with cumulative joint probability of precipitation and runoff using a copula function. Copulas are often used in multivariate frequency analysis, risk assessment, and drought modeling to simulate the dependency patterns of multivariate data (Aas et al., 2009; Hao & AghaKouchak, 2013; Hao et al., 2017; Laux et al., 2011; Ma et al., 2022). Negative MSDI denotes a dry climate, while positive MSDI denotes a wet climate. Hao and AghaKouchak (2013) and Hao et al. (2017) present more technical details on using copulas for multivariate joint distribution. Based on the US drought classification (Svoboda et al., 2002), MSDI or USDI ≥2.00 is exceptionally wet, between 1.60 and 1.99 is extremely wet, from 1.30 to 1.59 is severely wet, from 0.80 to 0.29 is moderately wet, 0.50 and 0.79 is abnormally wet, between −0.49 and 0.49 is normal, from −0.79 to −0.50 is abnormally dry, from −1.29 to −0.80 is moderate

drought, between −1.59 and −1.30 is severe drought, from −1.99 and −1.60 is extreme drought, and ≤−2.00 is exceptional drought. All drought index indicators were calculated on a 3-monthly scale.

2.3. Drought Attributes

Five drought attributes—severity, duration, intensity, and interarrival time—are examined for the historical and future periods under the two SSPs. The duration (DT in months) of a drought event (g) is the number of months in a row the SDI is less than −1 after being preceded and followed by values higher than 1. The cumulative effect of the drought episodes is the strength of the drought (drought severity, S) and is given as:

$$S_g = \sum_{z=1}^{DT} |\text{SDI}|$$ (1)

The ratio of the drought severity to the duration is the intensity of the drought. The period between the onsets of two subsequent drought episodes that fall under the same category is known as the drought's interarrival time. This describes how drought occurrences vary in their time. Drought propagation is based on how long it takes for the correlation between drought time series in different subsystems to reach its maximum value (Fuentes et al., 2022; Xu et al., 2019).

We examined the joint return period of drought events using a joint probability distribution function classified as either of the events exceeding specific values. The events considered were MSDI drought severity, duration, and intensity. We empirically determined the marginal distribution of each event to build the joint density functions and model the dependence structure between each event. Consequently, the copulas were calibrated against the empirical joint probability. The joint return period (R_{or}), where the continuous events W or Z or both exceed a prespecified threshold value (wp, zp), is given as (AghaKouchak et al., 2014; Hao et al., 2017):

$$R_{or} = \frac{\beta}{P(W \geq wp \, or \, Z \geq zp)} = \frac{\beta}{1 - C(a, b)}$$ (2)

where a and b are the marginal distribution of (W, Z). The average drought event's interarrival time is denoted by β.

2.4. Bias Correction of GCMs for Future Drought Projection

Many users seek high-resolution outputs to develop regional-to-local-scale climate predictions and climate impact assessments. However, this is challenging to achieve because of the coarse resolutions and inherent biases in GCMs. The inconsistencies between simulated and observed climatic variables are reduced through bias correction (BC). Since BC methods correct biases in different GCM aspects, the climate change signal must be preserved. Therefore, the effectiveness of four BC techniques—namely, univariate empirical quantile mapping (EQM), -quantile delta mapping (QDM), -scaling (SC), and multivariate bias correction employing an N-dimensional probability density function transform (MBCN) (Adeyeri et al., 2019, 2020c; Cannon, 2018; Dieng et al., 2022; Laux et al., 2021) were examined for both historical and future drought occurrences. Many correlated climate variables should be used for a robust multivariate BC approach. Hence, we utilized precipitation, minimum and maximum air temperature, relative humidity, wind speed, runoff, and mean air temperature for the multivariate bias correction. The best BC method was chosen based on the energy distance score during the historical period. The energy distance provides a theoretical underpinning for statistical inference and analysis, describing the equality of distributions (Rizzo & Székely, 2016). If the distributions are identical, the energy score is zero. This has been used in the climate model community to determine the accuracy of climate models (Adeyeri, Laux, Lawin, & Oyekan, 2020; Cannon, 2018). The detailed methodology flowchart is presented in Figure 1.

3. Results and Discussion

### 3.1. Spatiotemporal Spread and Bias Correction of Multimodel Drought Indicators

There are different spatial distributions for drought events in different years. For instance, Figure 2 presents the spatial distribution of the 2014 MSDI for the reference and CMIP6 models during the historical period.
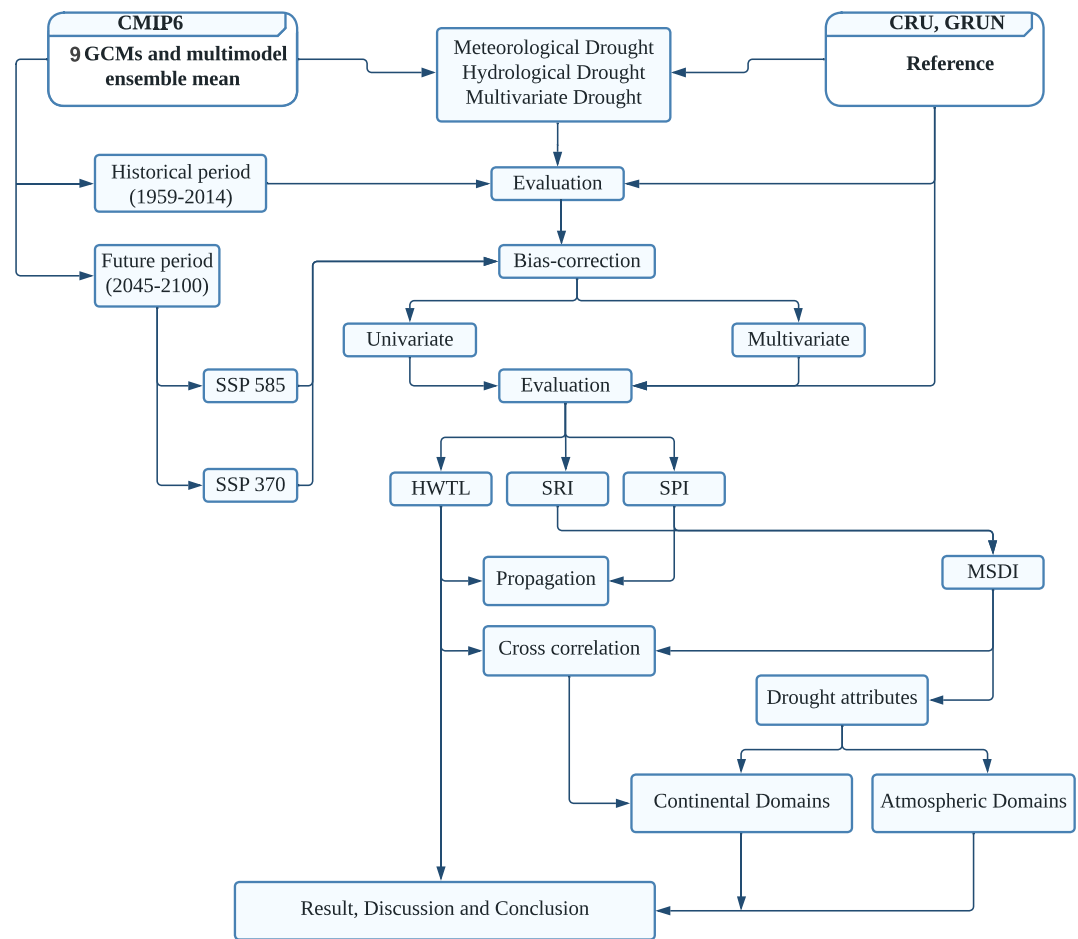
Figure 1. Workflow chart of the study.

All models misrepresent MSDI categories in most parts of the globe. For example, MRI and ENS simulated moderately wet conditions instead of normal conditions in Northwestern Russia. CMCC simulated extreme to exceptional drought conditions instead of normal to moderate drought in the Middle East. The varied land surface schemes, simulation of factors like vegetation and orography (Di Virgilio et al., 2022; Ehret et al., 2012), idealistic large-scale variability (Dieng et al., 2022), and divergent internal inconsistencies between climate models and observations could cause discrepancies (Adeyeri, Laux, Lawin, & Oyekan, 2020; Maraun, 2012). To quantify these inconsistencies, Figures S1–S3 in Supporting Information S1 show the root mean square error (RMSE) of the CMIP6 models for the MSDI, SRI, and SPI for 2014. For instance, CMCC and UKESM have high MSDI RMSE (>1.6) in the Sahel, while MRI and IPSL have high SRI RMSE (>3.0) in the same region. All models except IPSL recorded high SPI RMSE (>1.8) in the area. These inconsistencies could be caused by the models' inability to resolve the solar radiation accurately (Adeyeri et al., 2022), vegetation, cloud properties (Wild et al., 2005), or other synoptic-scale system interactions (Grose et al., 2019) of such locations.

To bolster these claims, a global temporal evaluation of the uncorrected ensemble mean model (Figure 3) shows the various misrepresentations of different droughts for the historical period (1959–2014). For example, Figure 3a shows that the raw model observed MSDI wet situations between 2011 and 2014; the reference shows various drought conditions. SRI also observed this pattern (Figure 3b), although with considerable differences in SPI (Figure 3c). Therefore, correcting the biases in the raw CMIP6 models is necessary to avoid misinterpreting drought episodes. The energy score for the different univariate and multivariate bias correction methods is presented in Figure 3d. A high energy score shows a wide mismatch between the distributions of participating series. For example, the raw CMIP6 model returned the highest value of 2.4, while the univariate EQM, SC, and QDM recorded less than 1. MBCN convergently recasts all attributes of the observed distribution to the CMIP6
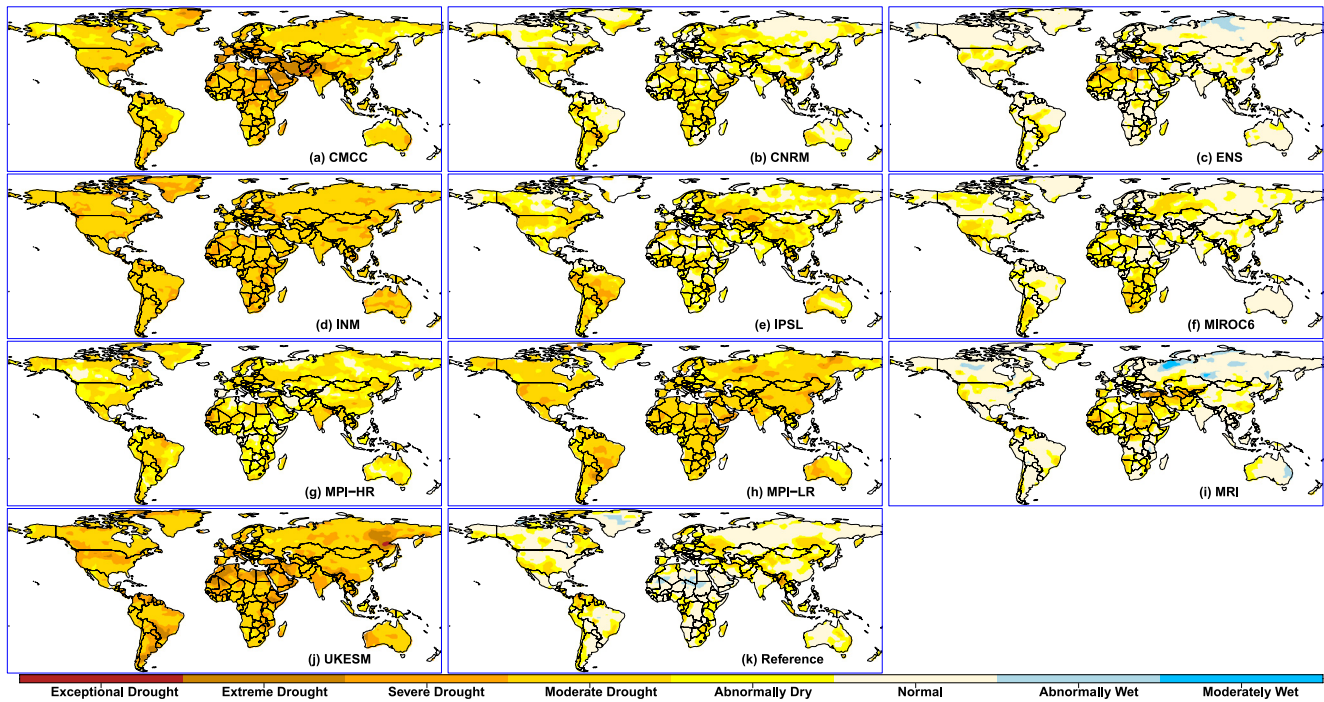
Figure 2. Spatial distribution of 2014 Multivariate Standardized Drought classification for the CMIP6 models (a-j) and reference (k).

simulations using iteratively rotational matrices (Adeyeri, Laux, Lawin, & Oyekan, 2020). This is indicated by the energy score for MBCN approaching zero after 20 iterations. Therefore, MBCN performed best in correcting the biases in the raw CMIP6 model. Many studies (Adeyeri, Laux, Lawin, & Oyekan, 2020; Cannon, 2018; Dieng et al., 2022) have shown that MBCN maintains the multivariate dependency structure needed for compound events. Consequently, the MBCN-corrected CMIP6 model was used in the subsequent sections.
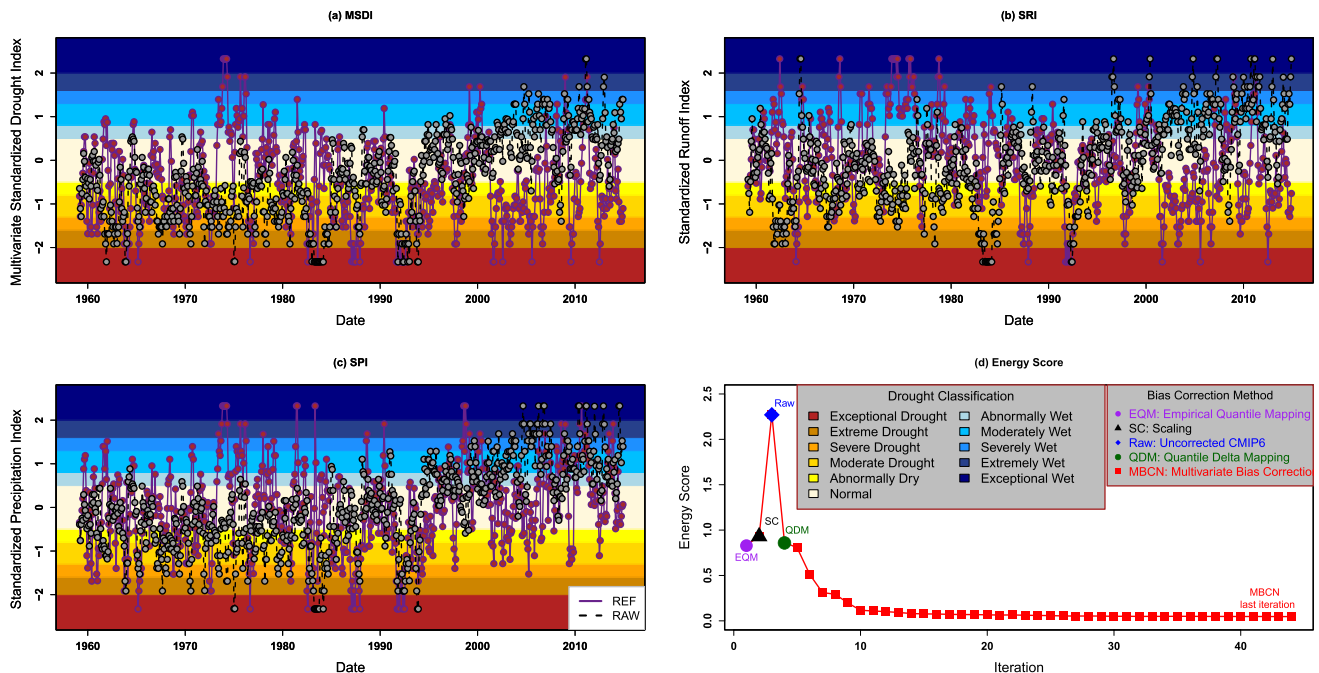
Figure 3. Distribution of drought classifications for observation and CMIP6 multimodel ensemble mean (a-c), and the energy distance for the raw and bias-corrected model using different methods(d). REF is the reference, and RAW is the uncorrected CMIP6 data. The background colours represent drought classifications.
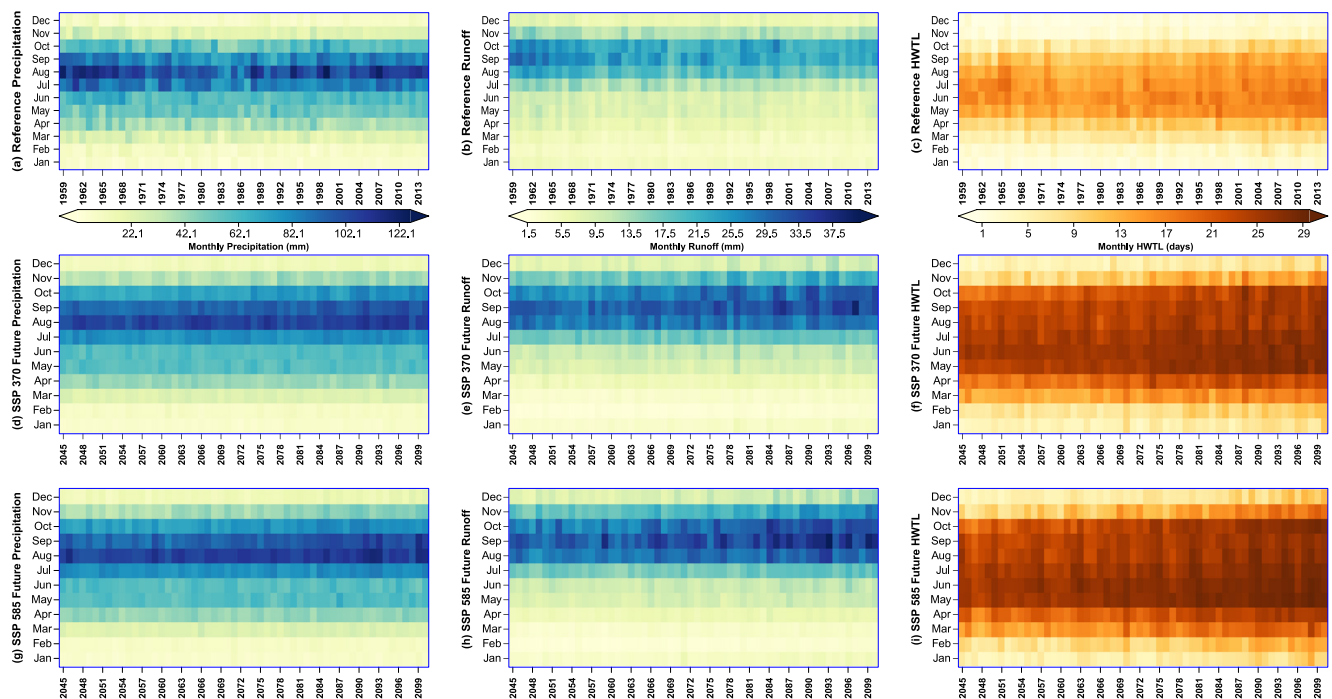
Figure 4. Temporal distribution of Precipitation (a, d, and g), Runoff (b, e, and h) and HWTL (c, f, and i) for Africa's tropical north domain for historical and future periods using the multivariate-bias-corrected CMIP6 multimodel ensemble mean.

To understand the relationship between drought variables, Figure 4 presents the historical and future temporal distribution of precipitation, runoff, and HWTL for Africa's tropical north region (as an example). The rainy season began in April and ended in October from 1959 to 2014, with a maximum of 122 mm of precipitation in August, the wettest month. November to March were the dry months; 1969 and 1997, particularly, had a few rainy days. The peak runoff occurred 1 month after the wettest month of the year (Figure 4b). Even though the wet season often begins in April, a substantial runoff was typically observed only in July.

For future projections under SSP 370 (Figure 4d), there was an increase in precipitation spread and intensity across months. For example, rainy season cessation shifted to November, and high precipitation intensity was recorded outside the historically wettest month. Consequently, the runoff regime was affected. The spread of peak runoff was elongated while the runoff volume also increased. Nevertheless, HWTL increased by up to 10 days/ month. This same pattern was observed under SSP 585, with different magnitudes. Also, HWTL increased in the wet season. This could be attributed to the concentration of relatively warm summer days (Pfleiderer et al., 2019). Furthermore, thermodynamic increases in the global mean temperature will cause these warm periods to intensify and create more lasting summer weather (Pfleiderer et al., 2019), thereby raising the danger of prolonged heatwaves, droughts, wet spells, and combined hot-dry extremes. Similarly, heavy precipitation events will be more intense, while soils will be more susceptible to drying out during warm weather due to global warming (Adeyeri, Laux, Lawin, Ige, & Kunstmann, 2020; Mann et al., 2018).

The drought indicators for the continental domains between 2010 and 2014 (Figure 5) demonstrate distinct categories for meteorological, hydrological, and multivariate droughts. For instance, 2011–2012 experienced both hydrological and multivariate droughts in Europe; there was no meteorological drought. Figure S4 in Supporting Information S1 shows the distribution for the entire historical period. Depending on the season under consideration, the onset of hydrological or multivariate drought could differ from that of meteorological drought and vice versa (Gebrechorkos et al., 2022). Figure S5 in Supporting Information S1 shows the future period between 2096 and 2100 under SSP 370. Over Asia, there was a constant transition between normal and wet episodes for all drought indices. Figure S6 in Supporting Information S1 shows the distribution for the entire future period. Figs. S7 and S8 in Supporting Information S1 show the indicators under SSP 585, while Figures S9–S11 in Supporting Information S1 show the drought distribution over the atmospheric circulation domains.
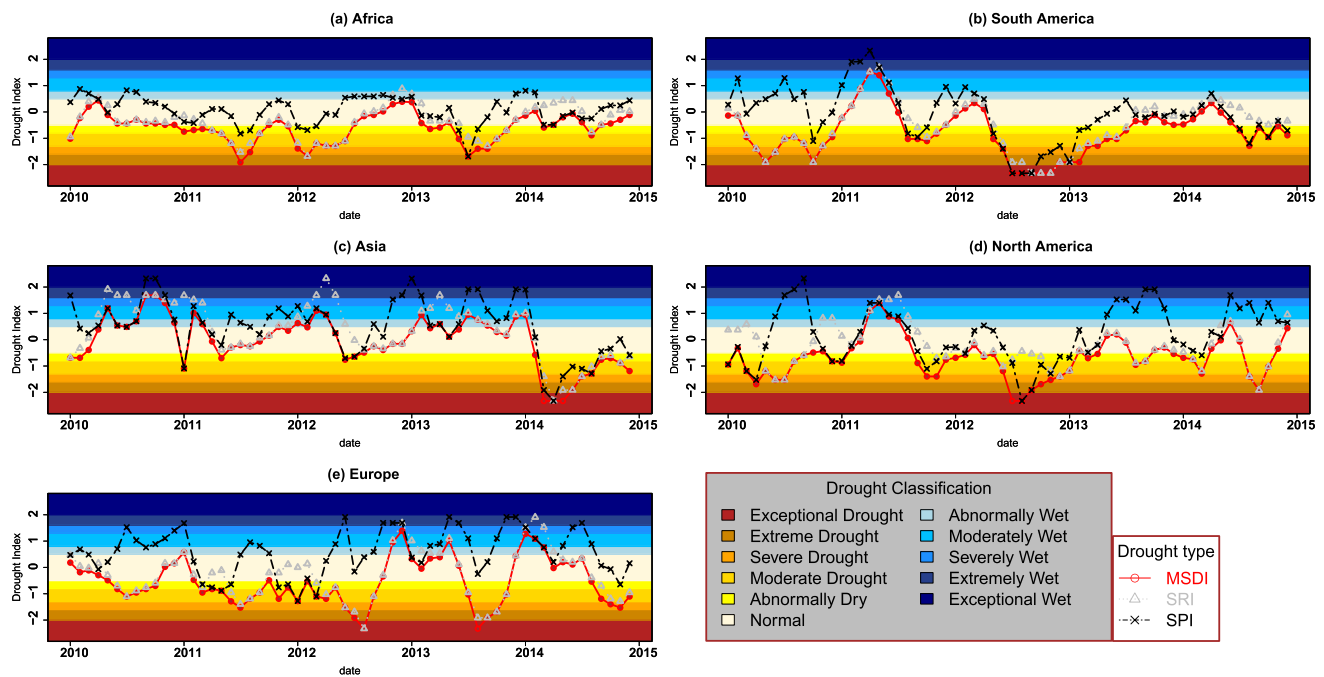
Figure 5. Univariate and multivariate drought indicators for continental domains between 2010 and 2014 using the reference series. The background colors represent drought classifications.

3.2. Cross Correlation Between HWTL and MSDI

Depending on the domain, heatwaves may not instantly lead to drought. Figure S12 in Supporting Information S1 clarifies the relationship between HWTL and the time-lagged MSDI. There were significantly high cross correlations for all lagged times between HWTL and MSDI in Africa and South America, indicating that HWTL was reasonably predictive of the subsequent multivariate drought events. This means that HWTL may increase MSDI during the first month of a lengthy heatwave because soil moisture deficits inhibit evaporative cooling and cloud formation during heatwaves (Donat et al., 2018; Pfleiderer et al., 2019). Similarly, in humid tropical regions (~30% in Africa and ~45% in South America), the cumulative effect of intense heatwaves can be exacerbated by persistently high humidity from evaporated water from wet soils over many days (Russo et al., 2017). As a result, there are highly significant correlations between Africa and South America. These correlations, however, weakened with lag time. This implies that episodes of prolonged heatwaves in previous months had little effect on the current MSDI. In Asia, the cross correlations increased with lag time, although at lag zero, the cross correlation was not significant. The low, nonsignificant correlations in North America could be attributed to the influence of melting ice sheets during heatwaves (Zhang et al., 2020), which replenishes the runoff; however, there are always lag times for the intersystem connections. This also agrees with Mazdiyasni and AghaKouchak (2015), who reported a nonsignificant drought trend despite the hiatus in the warming trend over the US.

3.3. Drought Severity, Intensity, and Interarrival Period

Regional disparities in dry/wet conditions can be seen on any given date because various dynamic variables influence drought attributes in space and time. Therefore, Figure 6 presents the historical MSDI drought characteristics between 1959 and 2014 for different continents.

Over Africa, the maximum severity (33.6) was observed between January 1983 and June 1984 (18-month duration), with an interarrival period of 19 months. This agrees with Henchiri et al. (2021), who reported the same over North and West Africa. The lowest severity (1.0) was observed in January 2010, with an interarrival period of 17 months. The maximum intensity (1.9) with a 14-month interarrival period was observed between August and November 1984, while the lowest intensity (1.0) was observed in January 2010. Between April 1987 and July 1988 (16 months), a maximum severity of 27.8 was recorded in North America, with a 22-month interarrival
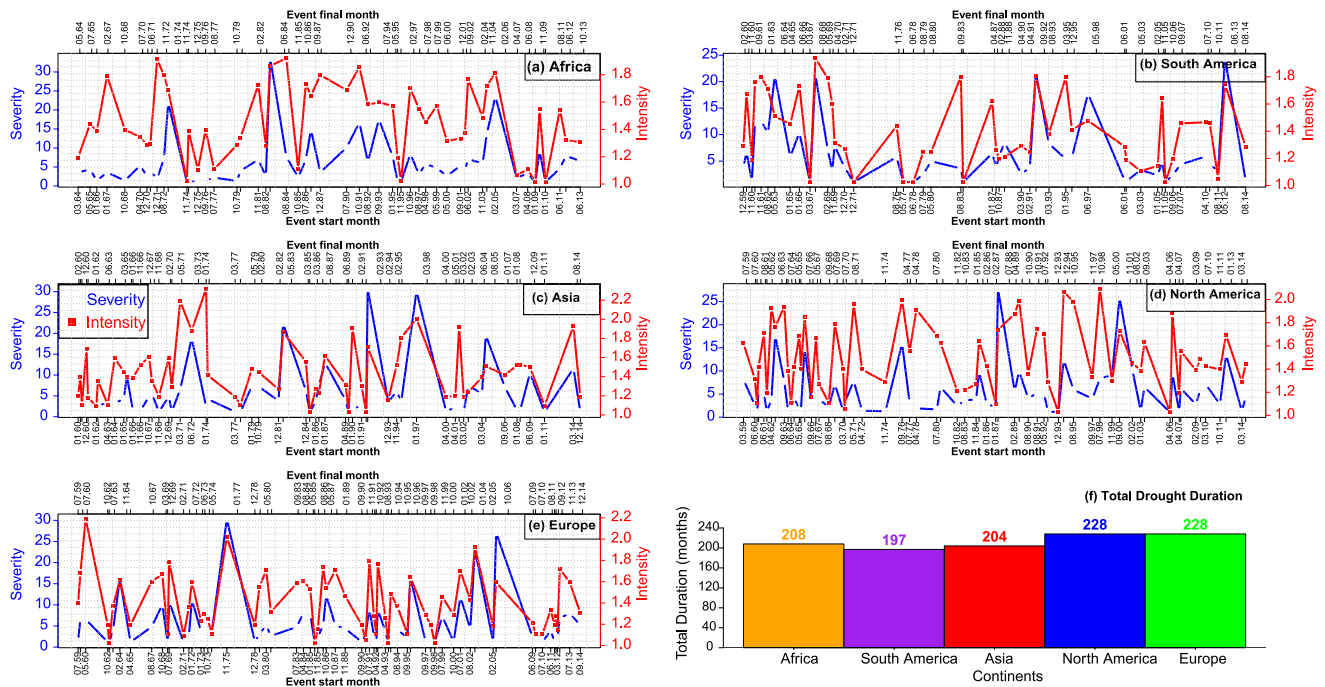
Figure 6. Historical drought characteristics between 1959 and 2014 for (a) Africa, (b) South America, (c) Asia, (d) North America, (e) Europe, and (f) total drought duration.

interval. An interarrival time of 3 months and the lowest severity (1.0) were both recorded in September 2006. From July–October 1998, there was a maximum intensity of 2.1 with a 16-month interarrival interval, and April 2006 saw the lowest intensity of 1.0.

The maximum severity of 30.3 was recorded in Europe between November 1975 and January 1977, while in Asia, the maximum severity of 30.7 was recorded between September 1991 and February 1993. The maximum intensity of 2.2 was recorded in Europe between May and July 1960, though in Asia, the maximum intensity of 2.3 was recorded in January 1974. This shows that maximum drought severity periods do not always correlate with drought intensity periods (Adhyani et al., 2017).

For the future projection under SSP 370 (Figure S13 in Supporting Information S1), Africa saw the maximum severity of 33.9 between May and December 2053, with an interarrival duration of 28 months. The 4-month interarrival time and the lowest severity of 1.1 were both recorded in October 2092. The lowest intensity of 1.1 was recorded in October 2092, while the highest intensity (2.3), with a 29-month intercorrecarrival duration, was recorded between August and September 2098. The maximum severity of 38.8 with a 23-month interarrival interval was seen in North America between July 2047 and February 2049. Also, August 2076 saw the lowest severity (1.0) and an interarrival time of 3 months. There was a maximum intensity of 2.0 with a 15-month interarrival period from March 2045 to April 2046, while August 2076 saw the lowest intensity of 1.0. Europe saw the most severity (23.6) between September 2046 and July 2047, whereas Asia experienced the highest severity (41.6) between September 2047 and May 2049, complimenting Nguyen et al. (2022). Between September 2046 and July 2047, Europe experienced its highest intensity (2.1), whereas Asia experienced its highest intensity (2.0) between September 2047 and May 2049. The projected changes in the global drought severity signal from historical to future generally agree with Tabari and Willems (2022) and Dai (2013).

Figure S14 in Supporting Information S1 shows the future drought attributes under SSP 585. In concert with Tabari and Willems (2022), all continents, except Europe, experienced increased severity from the historical to the future, with SSP 585 having the highest severity. The exception in Europe may be linked to wet soils, which impede land-atmosphere interactions in the projected MSDI (Pfleiderer et al., 2019). Contrary to Gebrechorkos et al. (2022), who observed the minimum drought duration in Europe using SPEI, the MSDI showed that Europe and North America generally saw the maximum MSDI drought duration (228 months), while South America
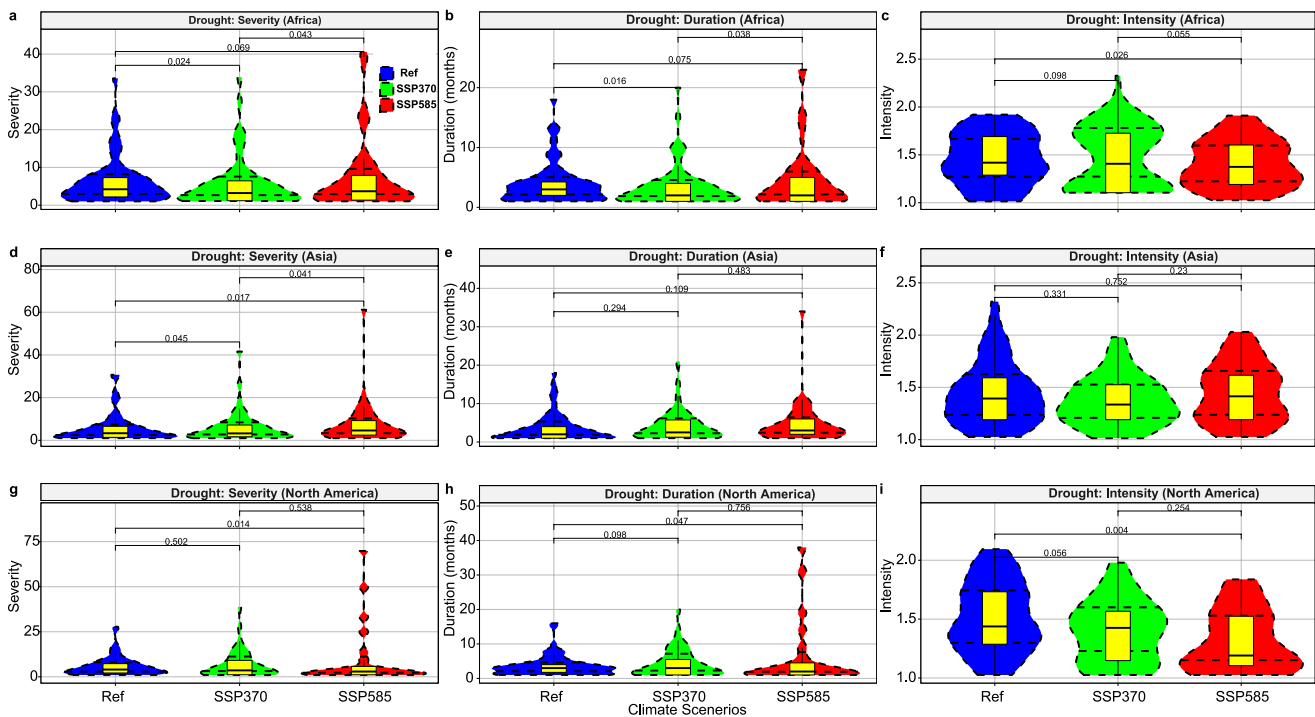
Figure 7. Statistical distribution and mean changes at 95% confidence interval of multivariate drought severity (a, d, and g), duration (b, e, and h), and intensity (c, f, and i) for Africa, Asia, and North America for the reference and future projection. Horizontal dotted lines represent 25% and 75% quartile ranges.

witnessed the minimum drought period (197) during the historical period. This is understandable because the two drought indicators are different. For future projections under SSP 370 and 585, Africa recorded the maximum drought duration (197 months), while Europe witnessed the minimum drought duration for SSP 370 (171 months), and North America (149 months) for SSP 585.

3.4. Distribution of Drought's Severity, Duration, and Intensity

The MSDI statistical summary (Figure 7) displays the various series distributions for the climate scenarios and continents. The estimated frequency of data points in each location correlates with the width of each density curve. Each density curve's peaks, troughs, and tails were examined to spot any patterns or differences across series. A broad density curve suggests that values in that range occur frequently, but a narrow density curve exhibits a low frequency of values in that range. Each situation has a different set of the previously listed features.

For instance, the severity displayed varying magnitudes, particularly in the various quantiles for the different continents. SSP 585's density curves also differed considerably from the other series. The mean changes were estimated with a 95% confidence level. Significant differences between the historical and SSP 370 MSDI severity means and between SSP 370 and 585 for MSDI severity means were seen across Africa. In Asia, there were no significant mean changes in any time slices for drought duration. However, the only significant difference in intensity mean in North America was seen between the historical and SSP-585 drought projections. In general, SSP 585 projections showed the highest severity and duration on all continents, while the historical period showed the highest intensity in Asia and North America. However, SSP 370 projections recorded the highest intensity in Africa.

3.5. Propagation

In addition to drought attributes, which may characterize drought effects on various subsystems, understanding drought propagation in different subsystems is essential for drought management. Figure 8 shows the heatwave and drought propagation during the historical period. In tropical Africa (Figures 8a(i)), the transition from meteorological to hydrological drought occurred more slowly during the wet months than during the dry months. For example, a meteorological drought in July will take 7 months to propagate into a hydrological drought. This is because there is enough subsurface flow to maintain streamflow (van Tiel et al., 2021). In addition, areas with
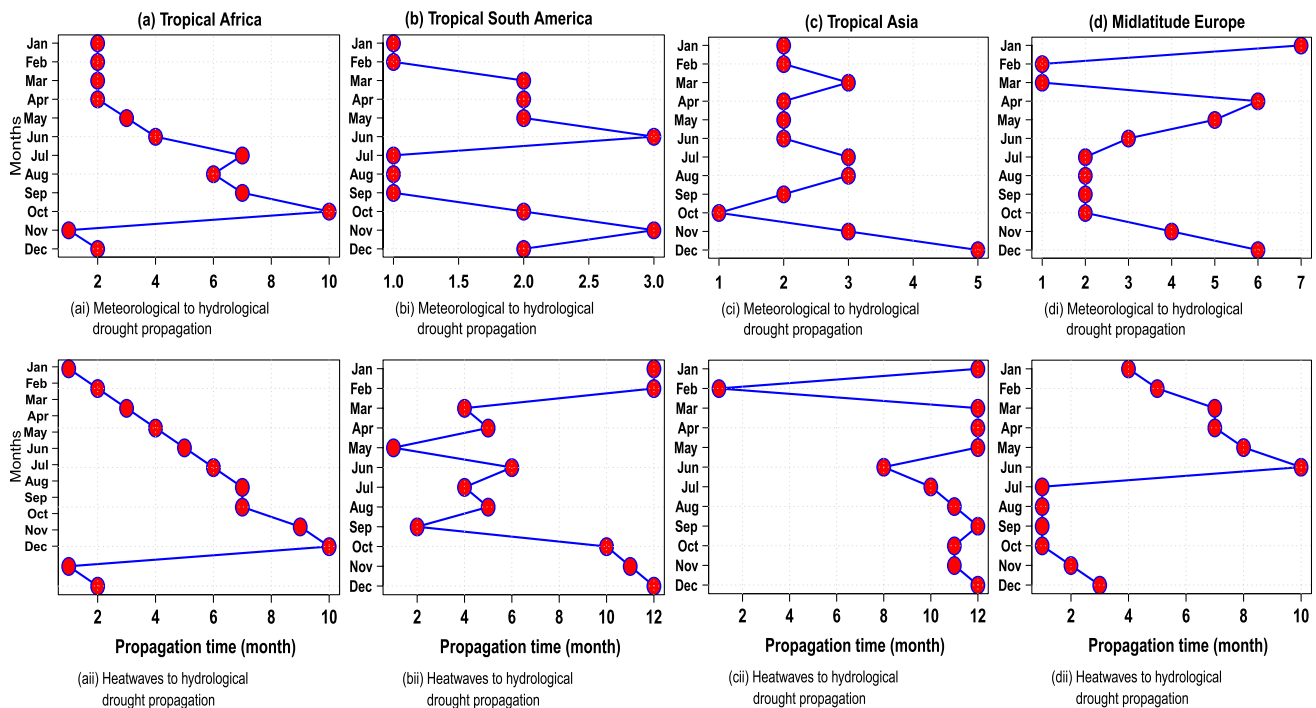
Figure 8. Heatwave and drought propagation during the historical period for (a) tropical Africa, (b) tropical South America, (c) tropical Asia, and (d) midlatitude Europe.

more forest cover will witness longer meteorological to hydrological drought propagation (Fuentes et al., 2022). Other considerations include climate, water management, and watershed features (Ding et al., 2021; Gebrechorkos et al., 2022). Additionally, it will take 10 months for heatwaves to propagate into a hydrological drought in October. This supports the evidence that heatwaves are abated by wet soils (Pfleiderer et al., 2019; Sutanto et al., 2020). Nevertheless, due to recharge and residence time delays, hydrological drought may have a longer propagation time (Gebrechorkos et al., 2022). In midlatitude Europe, the transition is more sinusoidal. The peak winter and spring months saw a delayed change from meteorological to hydrological drought. This may be related to the ice cover's effect or the melting current ice sheet (Zhang et al., 2020). However, during the summer, the transition was faster. The propagation of heatwaves to hydrological drought took an average of 1 month in the late summer and early autumn months.

For the projection period under SSP 370 and 585 (Figure 9), there were evident changes in drought propagation compared to the historical period. In tropical Africa under SSP 370 (Figure 9a(i)), there was a shift in the long period of meteorological-hydrological propagation from the middle and late wet months to the beginning of the wet months. In contrast, the late wet months exhibited a shorter propagation time. In the wet months, however, heatwave propagation into hydrological drought took 6–12 months. Under SSP 585, it took 2–4 months for a meteorological drought to propagate into a hydrological drought in the wet months. Furthermore, the propagation of heatwaves into a hydrological drought took 12 months. Likewise, over midlatitude Europe, the summer months were characterized by shorter meteorological-hydrological drought propagation under SSP 370. These shifts in the onset and cessation of heatwaves, droughts, and their associated properties may be attributed to climate change (Adeyeri, Laux, Lawin, & Oyekan, 2020; Naderi et al., 2022; Ridder et al., 2022; Sheffield et al., 2012). Generally, there is no universal propagation timing for drought events for the different continents and timescales, as this depends on the season, continent, and emission scenario (Cook et al., 2020). However, the uncertainty associated with using GCMs for drought propagation is reduced after bias correction, particularly by engaging a multivariate bias correction method. Consequently, drought propagation accuracy is improved.
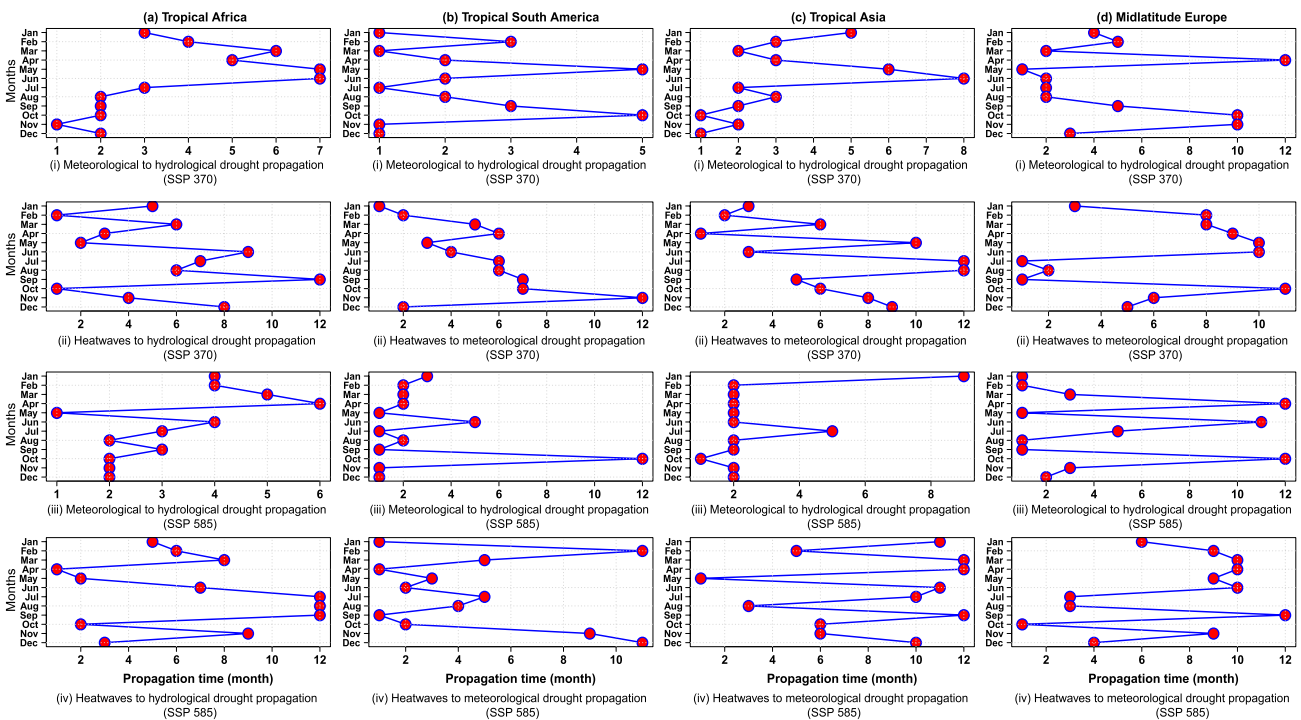
Figure 9. Heatwave and drought propagation during the future period under SSP 370 and 585 using the multivariate-bias-corrected CMIP6 multimodel ensemble mean (i) meteorological to hydrological drought propagation, (ii) heatwaves to hydrological drought propagation, (iii) heatwaves to hydrological drought propagation for (a) tropical Africa (b) tropical South America (c) tropical Asia and (d) midlatitude Europe.
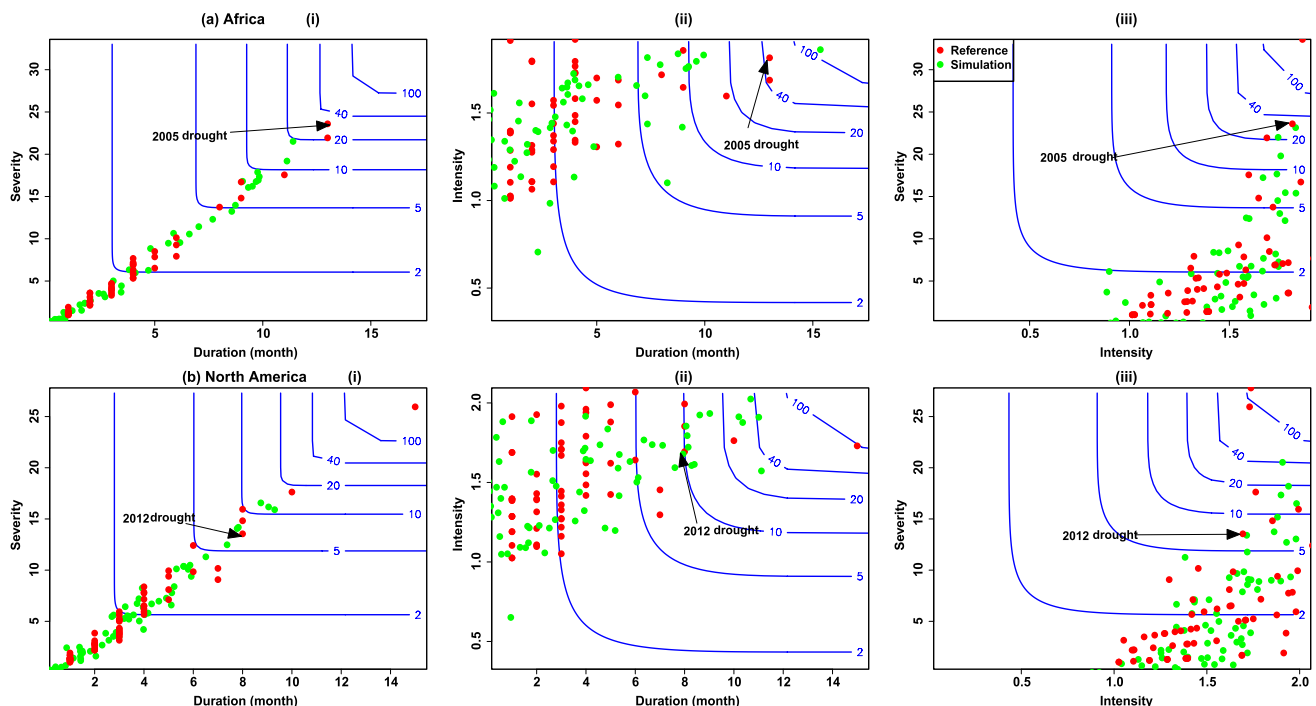
Figure 10. Joint return periods of multivariate drought (i) severity and duration, (ii) intensity and duration, (iii) severity and intensity for (a) Africa and (b) North America.

3.6. The Joint Probabilities and Return Period of MSDI Events

For multivariate risk analysis, the joint distribution is typically generated to derive the joint and conditional return periods of either of the events exceeding specific values. In the "OR" case scenario, Figure 10 shows the joint return periods of MSDI drought events as presented by joint copula distribution. First, the copula simulation (green) could simulate the observed distribution (red) quite well. This indicates that the copula captured the correlation structure regardless of the marginals. This agrees with Tabari and Willems (2022), who established that copula-based multivariate analysis gives a better knowledge of drought characteristics for more reliable drought forecasts.

In Figure 10a, the joint return period of severity and duration shows that the 2005 drought in Africa (severity 24 or duration 13 months) had a return period of around 33 years with a joint return probability of 97% (Figure S15a in Supporting Information S1). The joint return period of the 2005 drought's intensity (1.8) and duration shows a return period of 41 years with a joint return probability of 97.6%. However, the joint return period of the 2005 drought's intensity and severity is 36 years, with a joint return probability of 97%.

In North America, the 2012 drought (severity 44, or duration 8 months) had a return period of about 7 years with a joint return probability of 84% (Figure 10b and Figure S15b in Supporting Information S1). In contrast, the joint return period of the 2012 drought's intensity (1.7) and duration indicated a return period of 10 years with a joint return probability of 90%. However, the severity and intensity of the 2012 drought reveal a combined return period of 7 years with a joint return probability of 85%. Figures S16 and S17 in Supporting Information S1 show the joint return probabilities of future multivariate drought under SSP 370 and 585, respectively.

3.7. Possible Drought Drivers

The mechanisms driving various droughts and their spatiotemporal distribution may be complex and can also aggravate their intensities and impacts (Schubert et al., 2016). For instance, nonclimatic factors like large-scale groundwater extraction can interfere with drought propagation, thus exacerbating drought intensity (i.e., from meteorological to hydrological) or its impacts and severity (Ndehedehe et al., 2020). Nevertheless, large-scale climate teleconnection patterns and perturbations of the nearby oceans, including strong anomalies in sea surface temperature, have been well-established as critical drivers of drought variability (Hoerling et al., 2006; Park et al., 2016). Notable climate teleconnection patterns linked to various drought events include the El Niño-Southern Oscillation (ENSO) and Indian Ocean Dipole, among others (Chun et al., 2021; Ndehedehe et al., 2021). Globally, ENSO is a well-known index of oceanic variability that has been linked to variability in drought evolution in several climatic hotspots where drought frequency and severity are relatively higher. However, other low-frequency oscillations like the Atlantic Multidecadal Oscillation, Pacific Decadal Oscillation, and Atlantic Meridional Mode are also important large-scale climatic drivers of droughts across several subregions (Ndehedehe, 2022). Other drivers include Southern Annular Mode modifications, the mean sea level pressure, and the subtropical ridge (descending branch of the Hadley atmospheric cell) intensifications (van Dijk et al., 2013). Nonetheless, the interactions between these large-scale drivers and drought evolution differ across regions. Hence, future research could focus on the relationship between these interactions and regional to global drought events, especially to explore such interactions and drought impacts from a multivariate perspective.

4. Conclusions

Mitigating the effects of drought, especially in climate change, has become very important for planning, developing, and managing water resources. However, validating drought dynamics, variability, and trends within climate models is typically challenging but necessary for drought projections. Many studies have pointed out the shortcomings of climate models in simulating drought and have raised concerns about their usefulness for climate change applications because of the model uncertainties (Cook et al., 2020; McColl et al., 2022). We lessened the climate model uncertainty using nine distinct bias-corrected GCMs, and the multimodel ensemble mean. We emphasized the meteorological and hydrological droughts to simplify the drought categorization system and the MSDI to analyze the total hydrological-meteorological drought status. We observed different biases in the GCMs for the MSDI; however, the multivariate bias correction technique outperformed the other three methods in correcting these biases. Therefore, drought projections were based on the multivariate-bias-corrected climate models. Also, different drought indices gave different results for drought response. For example, the

meteorological drought response differs from the multivariate drought response. The HWTL-MSDI drought lag time also varied for each continent. Due to the variables' lagged reactions, it should be noted that a different drought propagation and response should be anticipated if a separate variable is chosen for drought. For instance, different behavior is expected if runoff is substituted for soil moisture. However, the MSDI accurately captured the times of previous drought episodes on several continents. Also, the copula captured the correlation of the joint dependency structure, regardless of the marginals. Therefore, this proves to be a dependable technique for establishing the relationships between drought events.

Even though our results show different drought characteristics and propagations for different regions, this can be generalized to incorporate additional subsystems, such as the economy, crop production, and agriculture. For most continents, more severe droughts are projected for the future, with greater severity under the SSP 585 scenario. This implies worsening future drought severity, making more countries vulnerable to climate change effects. Therefore, policymakers and planners must jointly consider the effects of drought on various subsystems, drought propagation properties, and regional climate attributes when developing drought preparedness, adaptation, or mitigation policies.

Data Availability Statement

The study's CMIP6 data used for global drought assessment are available through the Earth System Grid Federation at http://esgf.llnl.gov/.

The monthly reference data set series used for bias-correcting CMIP6 variables are archived by the Climate Research Unit (CRU) (Harris et al., 2020) of the University of East Anglia and The European Centre for Medium-Range Weather Forecasts (ECMWF) (Hersbach et al., 2020), and are publicly available on https://crudata.uea.ac.uk/cru/data/hrg/#info and https://cds.climate.copernicus.eu/#!/search?text=ERA5&type=dataset. The GRUN data used for the hydrological drought and the bias correction of CMIP6 runoff is archived by the Institute of Atmospheric and Climate Science, ETH, Zurich and publicly available via https://doi.org/10.6084/m9.figshare.9228176 (Ghiggi et al., 2021). All analyses and figures were drawn in the R Foundation for Statistical Computing version 4.2.2 Platform (https://cran.r-project.org/) and Python version 3.9 (https://www.python.org/).

References

Aas, K., Czado, C., Frigessi, A., & Bakken, H. (2009). Pair-copula constructions of multiple dependence. *Insurance: Mathematics and Economics*, *44*(2), 182–198. https://doi.org/10.1016/j.insmatheco.2007.02.001

Adeyeri, O. E., Akinsanola, A. A., & Ishola, K. A. (2017). Investigating surface urban heat island characteristics over Abuja, Nigeria: Relationship between land surface temperature and multiple vegetation indices. *Remote Sensing Applications: Society and Environment*, 7, 57–68. https://doi.org/10.1016/j.rsase.2017.06.005

Adeyeri, O. E., Laux, P., Lawin, A. E., & Arnault, J. (2020). *Assessing the impact of human activities and rainfall variability on the river discharge of Komadugu-Yobe Basin, Lake Chad Area* (Vol. 79). Environmental Earth Sciences.

Adeyeri, O. E., Laux, P., Lawin, A. E., Ige, S. O., & Kunstmann, H. (2020). Analysis of hydrometeorological variables over the transboundary Komadugu-Yobe basin, West Africa. *Journal of Water and Climate Change*, *11*(4), 1339–1354. https://doi.org/10.2166/wcc.2019.283

Adeyeri, O. E., Laux, P., Lawin, A. E., & Oyekan, K. S. A. (2020). *Multiple bias-correction of dynamically downscaled CMIP5 climate models temperature projection: A case study of the transboundary Komadugu-Yobe River Basin, lake Chad region, West Africa* (Vol. 2). SN Applied Sciences.

Adeyeri, O. E., Lawin, A. E., Laux, P., Ishola, K. A., & Ige, S. O. (2019). Analysis of climate extreme indices over the Komadugu-Yobe basin, Lake Chad region: Past and future occurrences. *Weather and Climate Extremes*, *23*, 100194. https://doi.org/10.1016/j.wace.2019.100194

Adeyeri, O. E., Zhou, W., Wang, X., Zhang, R., Laux, P., Ishola, K. A., & Usman, M. (2022). The trend and spatial spread of multisectoral climate extremes in CMIP6 models. *Scientific Reports*, *12*(1), 21000. https://doi.org/10.1038/s41598-022-25265-4

Adhyani, N. L., June, T., & Sopaheluwakan, A. (2017). Exposure to drought: Duration, severity and intensity (Java, Bali and Nusa Tenggara). *IOP Conference Series: Earth and Environmental Science*, *58*, 12040. https://doi.org/10.1088/1755-1315/58/1/012040

AghaKouchak, A., Cheng, L., Mazdiyasni, O., & Farahmand, A. (2014). Global warming and changes in risk of concurrent climate extremes: Insights from the 2014 California drought. *Geophysical Research Letters*, *41*, 8847–8852. https://doi.org/10.1002/2014GL062308

Agrafiotis, D. (2014). Video error Concealment. In D. R. Bull (Ed.), *Academic press library in signal processing. Volume 5: Image and video compression and multimedia* (pp. 295–321). Academic Press.

Ault, T. R. (2020). On the essentials of drought in a changing climate. *Science*, *368*(6488), 256–260. https://doi.org/10.1126/science.aaz5492

Ballarin, A. S., Barros, G. L., Cabrera, M. C., & Wendland, E. C. (2021). A copula-based drought assessment framework considering global simulation models. *Journal of Hydrology: Regional Studies*, *38*, 100970. https://doi.org/10.1016/j.ejrh.2021.100970

Cannon, A. J. (2018). Multivariate quantile mapping bias correction: An N-dimensional probability density function transform for climate model simulations of multiple variables. *Climate Dynamics*, *50*(1–2), 31–49. https://doi.org/10.1007/s00382-017-3580-6

Cheng, Y., Zhang, K., Chao, L., Shi, W., Feng, J., & Li, Y. (2023). A comprehensive drought index based on remote sensing data and nested copulas for monitoring meteorological and agroecological droughts: A case study on the Qinghai-Tibet plateau. *Environmental Modelling & Software*, *161*, 105629. https://doi.org/10.1016/j.envsoft.2023.105629

Chun, K. P., Dieppois, B., He, Q., Sidibe, M., Eden, J., Paturel, J.-E., et al. (2021). Identifying drivers of streamflow extremes in West Africa to inform a nonstationary prediction model. *Weather and Climate Extremes*, *33*, 100346. https://doi.org/10.1016/j.wace.2021.100346

Cook, B. I., Mankin, J. S., Marvel, K., Williams, A. P., Smerdon, J. E., & Anchukaitis, K. J. (2020). Twenty-first century drought projections in the CMIP6 forcing scenarios. *Earth's Future*, *8*, e2022JD037470. https://doi.org/10.1029/2019EF001461

Dai, A. (2013). Erratum: Increasing drought under global warming in observations and models. *Nature Climate Change*, *3*(2), 171. https://doi.org/10.1038/nclimate1811

Derradji, T., Belksier, M.-S., Bouznad, I.-E., Zebsa, R., Bengusmia, D., & Guastaldi, E. (2023). Spatio-temporal drought monitoring and detection of the areas most vulnerable to drought risk in Mediterranean region, based on remote sensing data (Northeastern Algeria). *Arabian Journal of Geosciences*, *16*, 1–17. https://doi.org/10.1007/s12517-022-11060-y

Di Virgilio, G., Ji, F., Tam, E., Nishant, N., Evans, J. P., Thomas, C., et al. (2022). Selecting CMIP6 GCMs for CORDEX dynamical downscaling: Model performance, independence, and climate change signals. *Earth's Future*, *10*, e2021EF002625. https://doi.org/10.1029/2021EF002625

Dieng, D., Cannon, A. J., Laux, P., Hald, C., Adeyeri, O., Rahimi, J., et al. (2022). Multivariate bias-correction of high-resolution regional climate change simulations for west Africa: Performance and climate change implications. *Journal of Geophysical Research: Atmospheres*, *127*, e2021JD034836. https://doi.org/10.1029/2021JD034836

Ding, Y., Xu, J., Wang, X., Cai, H., Zhou, Z., Sun, Y., & Shi, H. (2021). Propagation of meteorological to hydrological drought for different climate regions in China. *Journal of Environmental Management*, *283*, 111980. https://doi.org/10.1016/j.jenvman.2021.111980

Donat, M. G., Pitman, A. J., & Angélil, O. (2018). Understanding and reducing future uncertainty in midlatitude daily heat extremes via land surface feedback constraints. *Geophysical Research Letters*, *45*, 10627–10636. https://doi.org/10.1029/2018GL079128

Ehret, U., Zehe, E., Wulfmeyer, V., Warrach-Sagi, K., & Liebert, J. (2012). HESS opinions "Should we apply bias correction to global and regional climate model data?". *Hydrology and Earth System Sciences*, *16*(9), 3391–3404. https://doi.org/10.5194/hess-16-3391-2012

Eyring, V., Bony, S., Meehl, G. A., Senior, C. A., Stevens, B., Stouffer, R. J., & Taylor, K. E. (2016). Overview of the coupled model Inter-comparison project Phase 6 (CMIP6) experimental design and organization. *Geoscientific Model Development*, *9*(5), 1937–1958. https://doi.org/10.5194/gmd-9-1937-2016

Fuentes, I., Padarian, J., & Vervoort, R. W. (2022). Spatial and temporal global patterns of drought propagation. *Frontiers in Environmental Science*, *10*. https://doi.org/10.3389/fenvs.2022.788248

Gebrechorkos, S. H., Pan, M., Lin, P., Anghileri, D., Forsythe, N., Pritchard, D. M., et al. (2022). Variability and changes in hydrological drought in the Volta Basin, west Africa. *Journal of Hydrology: Regional Studies*, *42*, 101143. https://doi.org/10.1016/j.ejrh.2022.101143

Ghiggi, G., Humphrey, V., Seneviratne, S. I., & Gudmundsson, L. (2021). G-RUN ENSEMBLE: A multi-forcing observation-based global runoff reanalysis. *Water Resources Research*, *57*, e2020WR028787. https://doi.org/10.1029/2020WR028787

Grose, M. R., Foster, S., Risbey, J. S., Osbrough, S., & Wilson, L. (2019). Using indices of atmospheric circulation to refine southern Australian winter rainfall climate projections. *Climate Dynamics*, *53*(9–10), 5481–5493. https://doi.org/10.1007/s00382-019-04880-4

Guion, A., Turquety, S., Polcher, J., Pennel, R., Bastin, S., & Arsouze, T. (2022). Droughts and heatwaves in the Western Mediterranean: Impact on vegetation and wildfires using the coupled WRF-ORCHIDEE regional model (RegIPSL). *Climate Dynamics*, *58*(9–10), 2881–2903. https://doi.org/10.1007/s00382-021-05938-y

Han, Z., Huang, S., Huang, Q., Leng, G., Wang, H., Bai, Q., et al. (2019). Propagation dynamics from meteorological to groundwater drought and their possible influence factors. *Journal of Hydrology*, *578*, 124102. https://doi.org/10.1016/j.jhydrol.2019.124102

Hao, Z., & AghaKouchak, A. (2013). Multivariate standardized drought index: A parametric multi-index model. *Advances in Water Resources*, *57*, 12–18. https://doi.org/10.1016/j.advwatres.2013.03.009

Hao, Z., Hao, F., Singh, V. P., Ouyang, W., & Cheng, H. (2017). An integrated package for drought monitoring, prediction and analysis to aid drought modeling and assessment. *Environmental Modelling & Software*, *91*, 199–209. https://doi.org/10.1016/j.envsoft.2017.02.008

Harris, I., Osborn, T. J., Jones, P., & Lister, D. (2020). Version 4 of the CRU TS monthly high-resolution gridded multivariate climate dataset. *Scientific Data*, *7*(1), 109. https://doi.org/10.1038/s41597-020-0453-3

Henchiri, M., Igbawua, T., Javed, T., Bai, Y., Zhang, S., Essifi, B., et al. (2021). Meteorological drought analysis and return periods over North and West Africa and linkage with El Niño-southern oscillation (ENSO). *Remote Sensing*, *13*(23), 4730. https://doi.org/10.3390/rs13234730

Hersbach, H., Bell, B., Berrisford, P., Hirahara, S., Horányi, A., Muñoz-Sabater, J., et al. (2020). The ERA5 global reanalysis. *Quarterly Journal of the Royal Meteorological Society*, *146*(730), 1999–2049. https://doi.org/10.1002/qj.3803

Hoerling, M., Hurrell, J., Eischeid, J., & Phillips, A. (2006). Detection and attribution of Twentieth-century northern and southern African rainfall change. *Journal of Climate*, *19*(16), 3989–4008. https://doi.org/10.1175/JCLI3842.1

Iturbide, M., Casanueva, A., Bedia, J., Herrera, S., Milovac, J., & Gutiérrez, J. M. (2022). On the need of bias adjustment for more plausible climate change projections of extreme heat. *Atmospheric Science Letters*, *23*(2), e1072. https://doi.org/10.1002/asl.1072

Javed, T., Li, Y., Rashid, S., Li, F., Hu, Q., Feng, H., et al. (2021). Performance and relationship of four different agricultural drought indices for drought monitoring in China's mainland using remote sensing data. *The Science of the Total Environment*, *759*, 143530. https://doi.org/10.1016/j.scitotenv.2020.143530

Jehanzaib, M., & Kim, T.-W. (2020). Exploring the influence of climate change-induced drought propagation on wetlands. *Ecological Engineering*, *149*, 105799. https://doi.org/10.1016/j.ecoleng.2020.105799

Jiao, W., Wang, L., & McCabe, M. F. (2021). Multi-sensor remote sensing for drought characterization: Current status, opportunities and a roadmap for the future. *Remote Sensing of Environment*, *256*, 112313. https://doi.org/10.1016/j.rse.2021.112313

Laux, P., Rötter, R. P., Webber, H., Dieng, D., Rahimi, J., Wei, J., et al. (2021). To bias correct or not to bias correct? An agricultural impact modelers' perspective on regional climate model data. *Agricultural and Forest Meteorology*, *304–305*, 108406. https://doi.org/10.1016/j.agrformet.2021.108406

Laux, P., Vogl, S., Qiu, W., Knoche, H. R., & Kunstmann, H. (2011). Copula-based statistical refinement of precipitation in RCM simulations over complex terrain. *Hydrology and Earth System Sciences*, *15*(7), 2401–2419. https://doi.org/10.5194/hess-15-2401-2011

Le, P. V. V., Phan-Van, T., Mai, K. V., & Tran, D. Q. (2019). Space-time variability of drought over Vietnam. *International Journal of Climatology*, *39*(14), 5437–5451. https://doi.org/10.1002/joc.6164

Libonati, R., Geirinhas, J. L., Silva, P. S., Russo, A., Rodrigues, J. A., Belém, L. B. C., et al. (2022). Assessing the role of compound drought and heatwave events on unprecedented 2020 wildfires in the Pantanal. *Environmental Research Letters*, *17*(1), 15005. https://doi.org/10.1088/1748-9326/ac462e

Ma, J., Cui, B., Hao, X., He, P., Liu, L., & Song, Z. (2022). Analysis of hydrologic drought frequency using multivariate copulas in Shaying River Basin. *Water*, *14*(8), 1306. https://doi.org/10.3390/w14081306

Maity, R., Ramadas, M., & Govindaraju, R. S. (2013). Identification of hydrologic drought triggers from hydroclimatic predictor variables. *Water Resources Research*, *49*, 4476–4492. https://doi.org/10.1002/wrcr.20346

Mann, M. E., Rahmstorf, S., Kornhuber, K., Steinman, B. A., Miller, S. K., Petri, S., & Coumou, D. (2018). Projected changes in persistent extreme summer weather events: The role of quasi-resonant amplification. *Science Advances*, *4*(10), eaat3272. https://doi.org/10.1126/sciadv.aat3272

Maraun, D. (2012). Nonstationarities of regional climate model biases in European seasonal mean temperature and precipitation sums. *Geophysical Research Letters*, *39*, L06706. https://doi.org/10.1029/2012GL051210

Mazdiyasni, O., & AghaKouchak, A. (2015). Substantial increase in concurrent droughts and heatwaves in the United States. *Proceedings of the National Academy of Sciences of the United States of America*, *112*(37), 11484–11489. https://doi.org/10.1073/pnas.1422945112

McColl, K. A., Roderick, M. L., Berg, A., & Scheff, J. (2022). The terrestrial water cycle in a warming world. *Nature Climate Change*, *12*(7), 604–606. https://doi.org/10.1038/s41558-022-01412-7

Mukhawana, M. B., Kanyerere, T., & Kahler, D. (2023). Review of in-Situ and remote sensing-based indices and their Applicability for integrated drought monitoring in South Africa. *Water*, *15*(2), 240. https://doi.org/10.3390/w15020240

Naderi, K., Moghaddasi, M., & shokri, A. (2022). Drought occurrence probability analysis using multivariate standardized drought index and copula function under climate change. *Water Resources Management*, *36*(8), 2865–2888. https://doi.org/10.1007/s11269-022-03186-1

Naumann, G., Alfieri, L., Wyser, K., Mentaschi, L., Betts, R. A., Carrao, H., et al. (2018). Global changes in drought conditions under different levels of warming. *Geophysical Research Letters*, *45*(7), 3285–3296. https://doi.org/10.1002/2017gl076521

Ndehedehe, C. (2022). *Satellite remote sensing of Terrestrial Hydrology*. Springer International Publishing.

Ndehedehe, C. E., Agutu, N. O., Ferreira, V. G., & Getirana, A. (2020). Evolutionary drought patterns over the Sahel and their teleconnections with low frequency climate oscillations. *Atmospheric Research*, *233*, 104700. https://doi.org/10.1016/j.atmosres.2019.104700

Ndehedehe, C. E., Ferreira, V. G., Adeyeri, O. E., Correa, F. M., Usman, M., Oussou, F. E., et al. (2023). Global assessment of drought characteristics in the Anthropocene. *Resources, Environment and Sustainability*, *12*, 100105. https://doi.org/10.1016/j.resenv.2022.100105

Ndehedehe, C. E., Ferreira, V. G., Agutu, N. O., Onojeghuo, A. O., Okwuashi, O., Kassahun, H. T., & Dewan, A. (2021). What if the rains do not come? *Journal of Hydrology*, *595*, 126040. https://doi.org/10.1016/j.jhydrol.2021.126040

Ngcamu, B. S., & Chari, F. (2020). Drought influences on food isnsecurity in Africa: A systematic literature review. *International Journal of Environmental Research and Public Health*, *17*(16), 5897. https://doi.org/10.3390/ijerph17165897

Nguyen, N. B. P., Phan-Van, T., Trinh-Tuan, L. T., Tangang, F., Cruz, F., Santisirisomboon, J., et al. (2022). Projected future changes in drought characteristics over Southeast Asia. *Journal of Earth Sciences*, *44*, 127–143. https://doi.org/10.15625/2615-9783/16974

Nugraha, A. S. A., Kamal, M., Murti, S. H., & Widyatmanti, W. (2023). Development of the triangle method for drought studies based on remote sensing images: A review. *Remote Sensing Applications: Society and Environment*, *29*, 100920. https://doi.org/10.1016/j.rsase.2023.100920

O'Neill, B. C., Tebaldi, C., van Vuuren, D. P., Eyring, V., Friedlingstein, P., Hurtt, G., et al. (2016). The scenario model Intercomparison project (ScenarioMIP) for CMIP6. *Geoscientific Model Development*, *9*, 3461–3482. https://doi.org/10.5194/gmd-9-3461-2016

Park, J., Bader, J., & Matei, D. (2016). Anthropogenic Mediterranean warming essential driver for present and future Sahel rainfall. *Nature Climate Change*, *6*(10), 941–945. https://doi.org/10.1038/nclimate3065

Pfleiderer, P., Schleussner, C.-F., Kornhuber, K., & Coumou, D. (2019). Summer weather becomes more persistent in a 2°C world. *Nature Climate Change*, *9*, 666–671. https://doi.org/10.1038/s41558-019-0555-0

Ridder, N. N., Ukkola, A. M., Pitman, A. J., & Perkins-Kirkpatrick, S. E. (2022). Increased occurrence of high impact compound events under climate change. *NPJ Climate and Atmospheric Science*, *5*(1), 3. https://doi.org/10.1038/s41612-021-00224-4

Rizzo, M. L., & Székely, G. J. (2016). Energy distance. *Wiley Interdisciplinary Reviews: Computational Statistics*, *8*(1), 27–38. https://doi.org/10.1002/wics.1375

Russo, S., Sillmann, J., & Sterl, A. (2017). Humid heat waves at different warming levels. *Scientific Reports*, *7*(1), 7477. https://doi.org/10.1038/s41598-017-07536-7

Schubert, S. D., Stewart, R. E., Wang, H., Barlow, M., Berbery, E. H., Cai, W., et al. (2016). Global meteorological drought: A Synthesis of current understanding with a focus on SST drivers of precipitation deficits. *Journal of Climate*, *29*(11), 3989–4019. https://doi.org/10.1175/jcli-d-15-0452.1

Sheffield, J., Wood, E. F., & Roderick, M. L. (2012). Little change in global drought over the past 60 years. *Nature*, *491*(7424), 435–438. https://doi.org/10.1038/nature11575

Son, N. T., Chen, C. F., Chen, C. R., Chang, L. Y., & Minh, V. Q. (2012). Monitoring agricultural drought in the Lower Mekong Basin using MODIS NDVI and land surface temperature data. *International Journal of Applied Earth Observation and Geoinformation*, *18*, 417–427. https://doi.org/10.1016/j.jag.2012.03.014

Sutanto, S. J., Vitolo, C., Di Napoli, C., D'Andrea, M., & van Lanen, H. A. J. (2020). Heatwaves, droughts, and fires: Exploring compound and cascading dry hazards at the pan-European scale. *Environment International*, *134*, 105276. https://doi.org/10.1016/j.envint.2019.105276

Svoboda, M., LeComte, D., Hayes, M., Heim, R., Gleason, K., Angel, J., et al. (2002). The Drought Monitor. *Bulletin of the American Meteorological Society*, *83*(8), 1181–1190. https://doi.org/10.1175/1520-0477-83.8.1181

Tabari, H., & Willems, P. (2022). Trivariate analysis of changes in drought characteristics in the CMIP6 multimodel ensemble at global warming levels of 1.5°, 2°, and 3°C. *Journal of Climate*, *35*(18), 5823–5837. https://doi.org/10.1175/jcli-d-21-0993.1

van Dijk, A. I. J. M., Beck, H. E., Crosbie, R. S., de Jeu, R. A. M., Liu, Y. Y., Podger, G. M., et al. (2013). The Millennium Drought in southeast Australia (2001–2009): Natural and human causes and implications for water resources, ecosystems, economy, and society. *Water Resources Research*, *49*, 1040–1057. https://doi.org/10.1002/wrcr.20123

van Tiel, M., van Loon, A. F., Seibert, J., & Stahl, K. (2021). Hydrological response to warm and dry weather: Do glaciers compensate? *Hydrology and Earth System Sciences*, *25*(6), 3245–3265. https://doi.org/10.5194/hess-25-3245-2021

Wang, F., Wang, Z., Yang, H., Di, D., Zhao, Y., & Liang, Q. (2020). A new copula-based standardized precipitation evapotranspiration streamflow index for drought monitoring. *Journal of Hydrology*, *585*, 124793. https://doi.org/10.1016/j.jhydrol.2020.124793

Wild, M., Gilgen, H., Roesch, A., Ohmura, A., Long, C. N., Dutton, E. G., et al. (2005). From dimming to brightening: Decadal changes in solar radiation at Earth's surface. *Science (New York, N.Y.)*, *308*(5723), 847–850. https://doi.org/10.1126/science.1103215

Xu, B., Cardenas, M. B., Santos, I. R., Burnett, W. C., Charette, M. A., Rodellas, V., et al. (2022). Closing the global marine 226 Ra budget reveals the biological pump as a dominant removal flux in the upper ocean. *Geophysical Research Letters*, *49*, e2022GL098087. https://doi.org/10.1029/2022GL098087

Xu, L., Chen, N., Yang, C., Zhang, C., & Yu, H. (2021). A parametric multivariate drought index for drought monitoring and assessment under climate change. *Agricultural and Forest Meteorology*, *310*, 108657. https://doi.org/10.1016/j.agrformet.2021.108657

Xu, Y., Zhang, X., Wang, X., Hao, Z., Singh, V. P., & Hao, F. (2019). Propagation from meteorological drought to hydrological drought under the impact of human activities: A case study in northern China. *Journal of Hydrology*, *579*, 124147. https://doi.org/10.1016/j.jhydrol.2019.124147

Yuan, X., Zhang, M., Wang, L., & Zhou, T. (2017). Understanding and seasonal forecasting of hydrological drought in the Anthropocene. *Hydrology and Earth System Sciences*, *21*(11), 5477–5492. https://doi.org/10.5194/hess-21-5477-2017

Zhang, R., Sun, C., Zhu, J., Zhang, R., & Li, W. (2020). Increased European heat waves in recent decades in response to shrinking Arctic sea ice and Eurasian snow cover. *NPJ Climate and Atmospheric Science*, *3*(1), 7. https://doi.org/10.1038/s41612-020-0110-8